RSC Advances

ROYAL SOCIETY OF CHEMISTRY

www.rsc.org/advances

Journal Name

ARTICLE

Hexagonal ZnO nanorings: synthesis, formation mechanism and trimethylamine sensing properties

Received 00th January 20xx,
Accepted 00th January 20xx

DOI: 10.1039/x0xx00000x

www.rsc.org/

Chao Li,[a, b] Ying Lin,[a, b] Feng Li,[a, b] Linghui Zhu,[a, b] Dongming Sun,[b] Liang Shen,*[b] Yu Chen*[c] and Shengping Ruan*[a]

A one-step hydrothermal method assisted by polyvinylpyrrolidone (PVP) and polyviny akohol (PVA) was developed to synthesize hexagonal ZnO nanorings. X-ray diffractometer (XRD) and scanning electron microscopy (SEM) were used to characterized the as as-prepared ZnO nanorings and deduced the possible formation mechanism. The as-prepared ZnO nanorings showed the well-defined hexagonal shape with a width of 0.75 μm ~ 1.4 μm, a thickness of 0.17 μm ~ 0.33 μm and a hollow size of 0.2 μm ~ 1 μm. The trimethylamine (TMA) sensing performance of the hexagonal ZnO nanorings was tested. The results indicated that the hexagonal ZnO nanorings showed a high response (47 to 100 ppm TMA), fast response/recovery rate (less than 23 s and 37 s, respectively), wide linearity in a relatively wide range (1 ~ 200 ppm TMA), low detectable TMA minimum concentration (less than 5 ppm) and good selectivity to TMA. In addition, the TMA-sensing mechanism of the hexagonal ZnO nanorings was also discussed.

Introduction

With the improvement of people's life, seafood as an indispensable source of biologically valuable proteins, fats and fat-soluble vitamins, are extensively consumed all over the world. Consumption of spoiled seafood could cause serious health problems, such as septicemia and gastroenteritis, so detecting the freshness of seafood becomes a necessity in food industry.[1] Many research have shown that trimethylamine (TMA) can be used as an effective indicator of seafood quality because its content is increased with the decomposition of trimethyl-N-oxide in seafood after death.[2-4] In the evaluation of fish freshness, 0–10 ppm is regarded as fresh, and decay begins at over 10 ppm of TMA.[5] TMA as a malodorous gas existing in living or working environment is often released from fish-meal manufacturing process, wastewater treatment, waste disposal landfills, livestock farming, and hog manure.[6] Due to its potentially toxic and likely carcinogenic properties, TMA is considered as a strong environmental pollutant. TMA can irritate people's eyes and respiratory systems and has also been reported to inhibit the synthesis of macromolecules such as DNA, RNA and proteins and to have a teratogenic effect on animal embryos.[7] TMA is also observed in human exhaled breath as a result of an imbalance in the renal organ system and thus serves as the biomarker of renal diseases.[8]

So far, plenty of methods such as gas sensory evaluation, pH test, chromatography, high performance liquid chromatography, ion mobility spectrometry, and mass spectrometry etc., have been explored to analyze the content of TMA. However, among these methods, problems such as lack of accuracy, requires of complicated equipment, long sample preparation time, and professional operating skills are still difficult to overcome.[2] In contrast, gas sensors based on oxide semiconductors like ZnO, WO_3, SnO_2, MoO_3, and In_2O_3 etc, make it possible to realize cost-effective, rapid, reliable, nondestructive, on-site and real-time TMA analyzing.[2, 3, 5, 9-13]

Zinc oxide (ZnO), a n-type metal oxide semiconductor with a wide direct band gap (3.37 eV),[14] high exciton binding energy (60 meV)[15] and piezoelectricity[16] at room temperature, has been attracted great interest in catalysis,[17] photodetection,[18, 19] solar cell,[20] pressure transducer[21] and lithium ion battery[22] etc. In gas-sensing field, ZnO has been recognized as an excellent gas-sensing material for detection of toxic and harmful gas including TMA due to its biocompatibility, non-toxicity, stability, low-cost, ease of large scale fabrication and superior sensing properties.[23-28]

Recent years, because the performance can be tuned by the morphology,[29, 30] nano- and micro-scale ZnO with various morphologies such as zero-dimensional (0D) nanopaticles,[31] one-dimensional (1D) nanorods, nanowires and nanofibers,[32-34] two-dimensional (2D) nanoplates and nanosheets,[35, 36] and three-dimensional (3D) microspheres[37] etc. have been synthesized and investigated extensively. 1D and 2D

[a] State Key Laboratory on Integrated Optoelectronics, Jilin University, Changchun 130012, P. R. China.
E-mail: ruansp@jlu.edu.cn (S. Ruan)
[b] College of Electronic Science and Engineering, Jilin University, Changchun 130012, P. R. China.
E-mail: shenliang@jlu.edu.cn (L. Shen)
[c] Institute of Semiconductors, Chinese Academy of Sciences, Beijing 100083, P. R. China.
E-mail: chenyu_1099@163.com (Y. Chen)

† Electronic Supplementary Information (ESI) available: Sketch of gas sensor, EDS pattern and transient response curves See DOI: 10.1039/x0xx00000x

nanostructures, due to their large surface-to-volume ratio, better physical properties than conventional nanoparticles and high crystal structure etc., have been the new carriers for nanosensors and attracting great research interest in recent years.[38-40] Nanoring, as a specific 2D nanostructure, can be regarded as a 1D nanostructure bending into a 2D nanostructure in a plain and thus have the advantages of 1D and 2D nanostructures. What's more, the film based on nanorings exhibits the high accessible surface area and well-defined pore structure,[38, 41] which is favourable to the diffusion of target gases, thus resulting a good gas-sensing performance for gas-sensing material.

In this work, a one-step hydrothermal method was developed to synthesize ZnO nanorings with a well-defined hexagonal ring-like morphology. The subsequent TMA-sensing performance test indicated that the hexagonal ZnO nanorings based sensor was a good candidate for TMA detection due to its high response, fast response/recovery rate, low detectable TMA minimum concentration and good selectivity. Moreover, the formation mechanism and TMA-sensing mechanism of the hexagonal ZnO nanorings were also discussed.

Experimental section

Materials

All the starting agents were used without purification. Zinc nitrate hexahydrate ($Zn(NO_3)_2 \cdot 6H_2O$) and hexamethylenetetramine ($C_6H_{12}N_4$, HMTA) were purchased from the Xilong Chemical Co., Ltd. Polyvinyl alcohol 1788 (PVA-1788) and polyvinylpyrrolidone (PVP, K 88-96) were purchased from Aladdin chemistry Co., Ltd.

Preparation of hexagonal ZnO nanorings

The typical preparation of hexagonal ZnO nanorings are described as follows: 0.297 g $Zn(NO_3)_2 \cdot 6H_2O$, 0.35 g HMTA and 0.4 g PVP were successively dissolved in 20 mL deionized water under stirring at room temperature. When the PVP completely dissolved, a certain amount of PVA-1788 was added into above solution under stirring. After the PVA-1788 was dissolved completely, the resulting solution was gradually heated to 90 °C through the water bath and kept for 10 min under stirring. Then the resulting white suspension (the corresponding centrifugal products were denoted as Product-A) was transferred into a 30 mL Teflon-lined stainless steel autoclave for hydrothermal treatment at 90 °C for 6 h. After cooling down to room temperature, the products (denoted as Product-B, and can be prove to be hexagonal ZnO nanorings below) were rinsed with hot deionized water several times followed by drying in air at 60 °C overnight. The synthetic processe is shown Fig. 1.

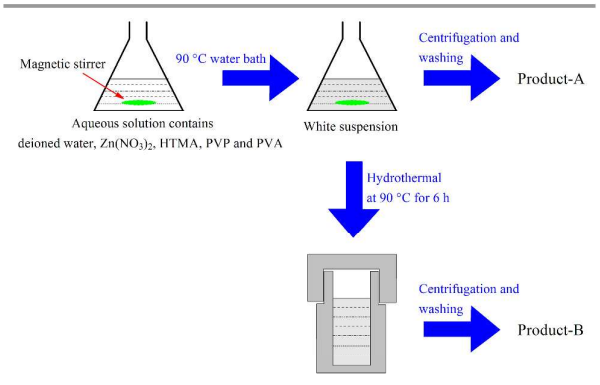

Fig. 1. Synthetic process of the hexagonal ZnO nanoplates (Product-A) and ZnO nanorings (Product-B).

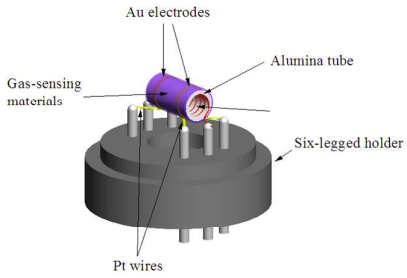

Fig. 2. Sketch of gas sensor.

Characterization

The sample were characterized by powder X-ray diffractometer (XRD, Shimadzu XRD-6000 with Cu Kα radiation, λ = 0.154178 nm) and scanning electron microscopy (SEM, JSM6700F).

Gas sensor fabrication and test

The fabricating process of sensors in brief: The as-prepared ZnO were mixed with deionized water in a weight ratio of 100: 25 to form a paste. The paste was coated onto a ceramic tube on which a pair of gold electrodes was previously printed, and then a Ni-Cr heating wire was inserted in the tube to form a side-heated gas sensor. The fabricated sensor is shown in Fig. 2.

Gas sensing properties were measured by a CGS-8 (Chemical gas sensor-8) intelligent gas sensing analysis system (Beijing Elite Tech Co. Ltd., China). The gas response was defined as S = Ra/Rg, where the Rg and Ra are the resistance values of sensors in the presence and absence of the target gas, respectively. The time taken by the sensor to achieve 90% of the total resistance change was defined as the response time in the case of adsorption or the recovery time in the case of desorption. The detectable minimum is defined as the concentration makes the response of sensor reach to 3.

Results and discussion

Fig. 3 shows the XRD patterns of the Product-A and Product-B. Compared with the data in JCPDS No. 36-1451, all the peaks in the patterns can be indexed to hexagonal wurtzite ZnO. And it

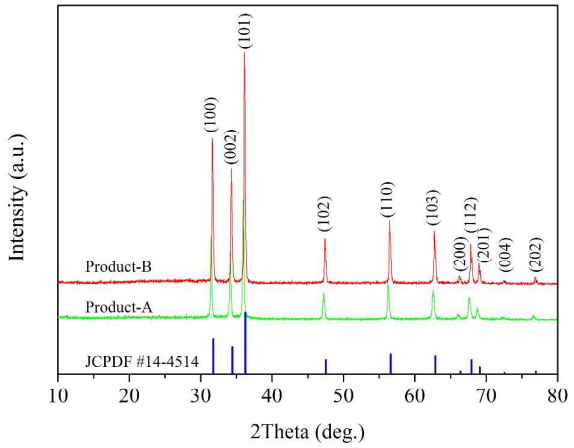

Fig. 3. XRD patterns of Product-A and Product-B.

proves that both Product-A and Product-B were ZnO. A closer examination reveals the diffraction peaks shifts to small angle, indicating the lattice parameters of Product-A is bigger than those of the normal ZnO due to the rapid formation. In addition, no other characteristic peaks for impurity are observed.

The SEM images of the Product-A and Product-B are shown in Fig. 4 (a) and (b), and the inserts show the corresponding high-magnification SEM images. It can be seen that the Product-A, obtained after the 90 °C water bath treatment,

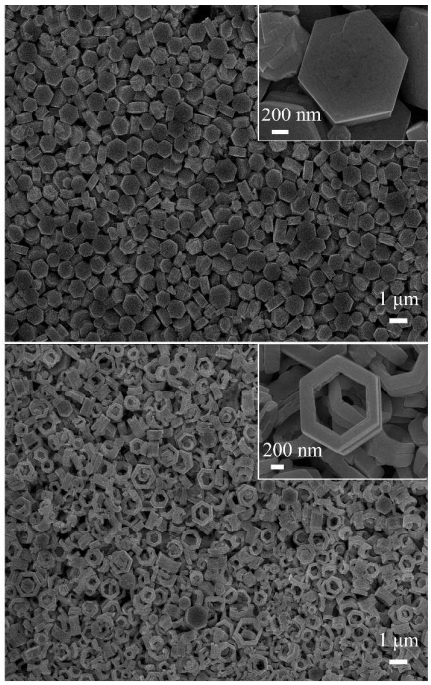

Fig. 4. Low- and high-magnification SEM images of (a) the Product-A and (b) Product-B.

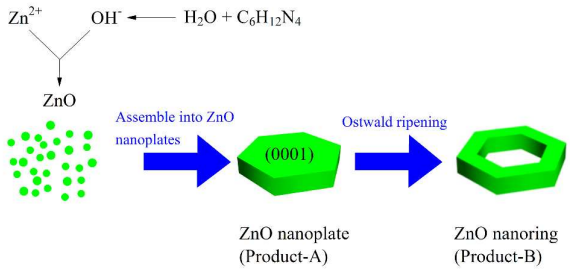

Fig. 5. Formation process of the hexagonal ZnO nanoplates and nanorings.

shows a hexagonal plate-like morphology with a width of 0.7 μm ~ 1.2 μm and a thickness of 0.21 μm ~ 0.29 μm. While the Product-B, obtained after the 90 °C hydrothermal process for 6 h, show a hexagonal ring-like morphology with a width of 0.75 μm ~ 1.4 μm, a thickness of 0.17 μm ~ 0.33 μm and a hollow size of 0.2 μm ~ 1 μm. The porous morphology of the hexagonal ZnO nanorings can facilitate the diffusion and distribution of surrounding gas phase to the surface of the internal ZnO, which will contribute to improving the gas sensing properties greatly. In addition, both the hexagonal ZnO nanoplates (i.e. Procuct-A) and hexagonal ZnO nanorings (i.e. Procuct-B) were in pairs.

Here, according to the results of XRD and SEM, it can be deduced that the Product-A is plate-like ZnO while Product-B is ring-like ZnO. And the possible formation mechanism of the hexagonal ZnO nanorings is as following. When the precursor solution is heated to and maintained at 90 °C, HMTA hydrolyzes gradually and it makes the solution be alkaline. Then Zn^{2+} combined with OH- resulting ZnO nanoparticles rapidly at 90 °C. At the same time, to reduce the surface energy, these ZnO nanoparticles rapidly assemble into hexagonal ZnO nanoplates. The corresponding reactions are shown as below:[42]

$$(CH_2)_6N_4 + 6\ H_2O \rightarrow 6\ HCHO + 4\ NH3 \quad (1)$$

$$NH3 + H2O \rightarrow NH^{4+} + OH^- \quad (2)$$

$$Zn(NO_3)_2 + H_2O \rightarrow Zn^{2+} + 2\ HNO_3 \quad (3)$$

$$2\ OH^- + Zn^{2+} \rightarrow ZnO(s) + H_2O \quad (4)$$

During the following hydrothermal process, the hexagonal ZnO nanolates gradually transform into hexagonal ZnO nanorings via Ostwald ripening. PVP and PVA in the solution play the key roles in inhibiting the growth of ZnO along (0001) direction and hollowing ZnO nanoplate. Both PVP and PVA are capping agents and used to control the shape and size of metal oxide.[43, 44] PVP and PVA can adsorbed on the surface of ZnO nanoparticle especially the polar {0001} facets of ZnO,[45] resulting a plate-like ZnO when the precursor solution was heated to 90 °C and the formation of ZnO nanorings through Ostwald rippenning during the hydrothermal treatment. The sketch of formation process of the hexagonal ZnO nanorings is shown in Fig. 5.

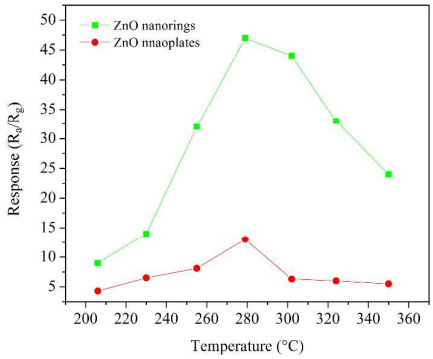

Fig. 6. Responses of hexagonal ZnO nanoplates and nanorings to 100 ppm TMA as a function of the operating temperature.

In order to find the optimum operating temperature of the sensors based on the hexagonal ZnO nanoplates and nanorings, their responses to 100 ppm TMA at different operating temperature (from 205 to 350 °C) were collected. As shown in Fig. 6, the responses of the two sensors to TMA increase with the augment of operating temperatures and attain their maximum values both at 280 °C, followed by decreases. And the ZnO nanorings show a much higher response of 47 than that of ZnO nanoplates (13) at 280 °C. So, 280 °C was chosen as their optimal operating temperature and the following gas-sensing performance was tested at this temperature.

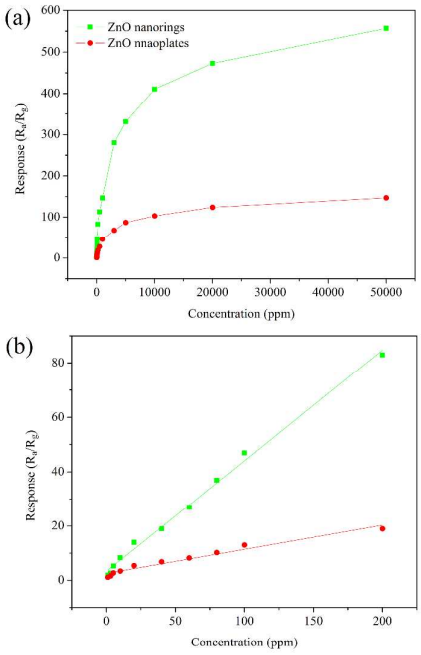

Fig. 7. (a) Response curves as a function of trimethylamine concentration and (b) linear response towards 1 ppm to 200 ppm TMA of the hexagonal ZnO nanoplates and nanorings at 280 °C.

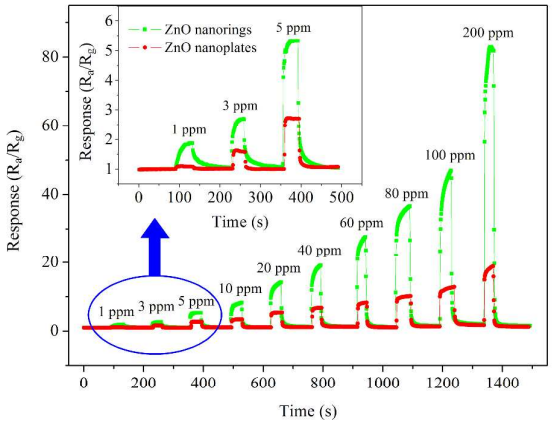

Fig. 8. Transient responses of the hexagonal ZnO nanoplates and nanorings to 1, 3, 5, 10, 20, 40, 60, 80, 100 and 100 ppm TMA at 280 °C.

The responses of the hexagonal ZnO nanoplates and nanorings to different concentrations of TMA at the optimal operating temperature are shown in Fig. 7. It can be easily found from Fig. 7(a), that the responses of the two sensors increase rapidly with increasing of the TMA concentration, and then gradually slow down, but do not reach saturation until 50000 ppm. Compared with ZnO nanoplates, ZnO nanorings show the highly enhanced response to each concentration of TMA. What's more, as shown in Fig. 7(b), the responses of the two sensors both exhibit approximately linear increase from 1 to 200 ppm. In addition, the detectable TMA minimum concentration is between 3 ppm and 5 ppm for ZnO nanorings (the corresponding responses were about 2.7 and 5.3, respectively). While, the detectable TMA minimum concentration for ZnO nanoplates is between 5 ppm and 10 ppm (the corresponding responses were 2.7 and 3.4, respectively).

As for gas sensing application, rapid response and recovery is of great importance to real-time monitor. To investigate the response-recovery behaviors of the hexagonal ZnO nanoplates and nanorings, the sensors were sequentially exposed to 1, 3, 5, 10, 20, 40, 60, 80, 100 and 200 ppm TMA at the optimal operating temperature. As shown in Fig. 8, when the sensor exposed to TMA the response increases rapidly and when subjected to air the sensors' recovery to the initial state is also rapid. The response time and recovery time of ZnO nanorings are within 23 s and 37 s, respectively. While, the response time and recovery time of ZnO nanorings are within 10 s and 8 s, respectively. Compared with ZnO nanoplates, the longer response/recovery time of ZnO nanorings can be explained as following: although a better porosity is good for gas diffusion and thus enhances sensor's response, it remains need enough time for the tested gas (TMA) to diffuse into the deep sensing film and for the produced gases (CO_2, H_2O and N_2) to diffuse out of the deep sensing film. The ZnO nanorings have more pores and higher response (means more reacted TMA and produced gases) than the ZnO nanoplates, and as a result longer response/recovery time is needed.

Table 1. Comparisons of TMA sensors in this work and some reported literatures.

Materials		Method	Operating temperature	response	Response/recovery time	Detectable limit
ZnO nanosheets[46]		Hydrothermal	260 °C	About 3.7 (100 ppm)	5.4 s / 32.8 s (50 ppm)	About 50 ppm
Fe_2O_3-nanorod-decorated ZnO nanosheets[46]		Two-step hydrothermal	260 °C	About 8.4 (100 ppm)	0.7 s / 7.1 s (50 ppm)	< 20 ppm
ZnO thin film[47]		Spray pyrolysis	30 °C	4.7 (50 ppm)	15 s / 14 s	About 40 ppm
Punched ZnO nanobelt[25]		Vapor-phase growth and thermal annealing	400 °C	40 (5 ppm)	---[a]	About 0.05 ppm
α-Fe_2O_3 nanorods/TiO_2 nanofibers[48]		Electrospinning and hydrothermal	250 °C	33.1 (100 ppm)	0.5 s / 1.5 s (100 ppm)	---
Thoria-incorporated SnO_2[49]		Sintering	225 °C	1500 (800 ppm)	15 s / 20 min	---
WO_3 thin film[50]		Sol–gel technique	70 °C	About 15 (100 ppm)	3.5 s / 21 s	50 ppm
This work	ZnO nanorings	Hydrothermal	280 °C	47 (100 ppm)	19 s / 8 s (100 ppm)	< 5 ppm
This work	ZnO nanoplates	90 °C water bath treatment	280 °C	13 (100 ppm)	6 s / 4 s (100 ppm)	< 10 ppm

[a] The short line presents the corresponding data is not spelled out in the literature.

The gas sensing selectivity is another important parameter to evaluate the sensing ability of oxide semiconductor materials. Fig. 9 shows the cross-sensitivities of the hexagonal ZnO nanoplates and nanorings to 100 ppm various gases including ammonium (NH_3), carbon monoxide (CO), xylene (C_8H_{10}), formaldehyde (HCHO), acetylene (C_2H_2), acetone (CH_3COCH_3), ethanol (C_2H_5OH) and TMA. It is clear that the hexagonal ZnO nanoplates and nanorings exhibit the largest responses towards TMA among the tested gases and the ZnO naorigns show a better selectivity to TMA than the ZnO nanoplates. Such a result indicates that the hexagonal ZnO nanorings exhibit an excellent selectivity towards TMA against the other tested gases at the optimal operating temperature of 280 °C.

Comparisons among ZnO nanoplates, ZnO nanorings and other reported TMA-sensing materials are displayed in Table 1. As can be seen, the ZnO nanorings have an advantage in detecting TMA due to the relative high response, low detectable limit, fast response/recovery speed as well as simple synthetic method.

The TMA sensing mechanism of the hexagonal ZnO nanorings can be explained as follows and illustrate in Fig. 10(a) - (c). Fig. 10(a) shows sketch of the porous TMA-sensing film composed by the hexagonal ZnO nanorings and Fig. 10(b) illustrate the electronic transmission path within and between ZnO nanoring(s). Response of semiconducting metal oxides is based on the reactions between target gas molecule and the oxygen species on the surface of oxides [51, 52]. As shown in Fig. 10(c), when the hexagonal ZnO nanorings are surrounded by air, oxygen molecules can be adsorbed on their surface to generate chemisorbed oxygen species by capturing electrons from the conduction band of ZnO. As a result, a wide depletion layer generates and it narrows the electronic transmission channel, which can lead to a decrease in ZnO nanorings' conductivity. When the sensor is exposed to TMA, TMA molecules can react with the chemisorbed oxygen species (O^- is believed to be dominant at 280 °C[53, 54]) and release the trapped electron back to the conduction band, which will increase the carrier concentration, narrow the depletion layer, widen the electronic transmission channel and result in the reducing of ZnO nanorings' resistance. The reaction between surface oxygen species and TMA can be simply described as [4]:

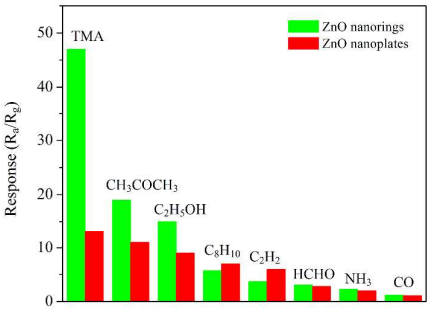

Fig. 9. Selectivity of the hexagonal ZnO nanoplates and nanorings at 280 °C

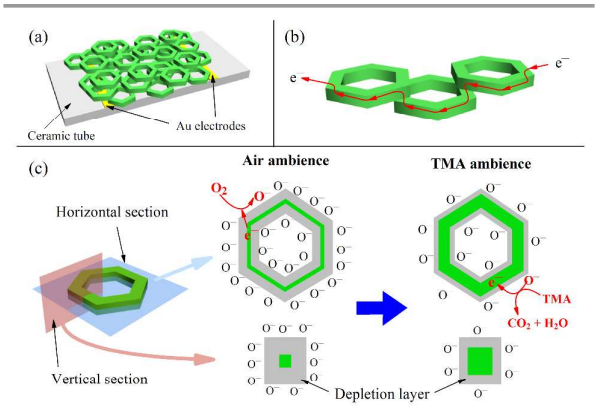

Fig. 10. (a) Local sketch of the porous TMA-sensing film composed by the hexagonal ZnO nanorings; (b) the electronic transmission path within and between ZnO nanoring(s); (c) TMA-sensing mechanism of the hexagonal ZnO nanorings.

$$2\ N(CH_3)_3 + 21\ O^- = N_2 + 9\ H_2O + 6\ CO_2 + 42\ e^- \quad (1)$$

In addition, the porous structure of the TMA-sensing film composed by ZnO nanorings is beneficial to gas diffusion and provides more active sites for oxygen adsorption and the reaction between adsorbed oxygen species and TMA, which also contributes to the high response and rapid response/recovery rate.

Conclusions

In conclusion, a facile one-step hydrothermal method was developed to synthesize the hexagonal ZnO nanorings. The XRD and SEM results revealed that the formation of the hexagonal ZnO nanorings could be attributed to the Ostwald ripening process assisted by PVP and PVA. The as-synthesized hexagonal ZnO nanorings were used to fabricate the sensor for TMA detection and the test results indicated that the sensor exhibited the excellent TMA-sensing properties at 280 °C. Typically, the response to 100 ppm TMA was 47, the response and recovery time were 19 s and 8 s respectively and detectable TMA limit was about 3 ppm. In addition, the sensor showed a good linearity and selectivity to TMA which also make it a candidate for practical TMA-sensing application.

Acknowledgements

This work was supported by the National Natural Science Foundation of China (Grant Nos. 61404058 and 61274068), Chinese National Programs for High Technology Research and Development (Grant No. 2013AA030902), Project of Science and Technology Plan of Changchun City (Grant No. 14KG020) and Opened Fund of the State Key Laboratory on Integrated Optoelectronics (No. IOSKL2013KF10).

Notes and references

1 I.N.A. Ashie, J.P. Smith, B.K. Simpson and D.N.F. Haard, *Crit. Rev. Food Sci.*, 1996, **36**, 87.
2 J.Y. Jung and C.S. Lee, *J. Ind. Eng. Chem.*, 2011, **17**, 237-242.
3 X.F. Chu, S.M. Liang, W.Q. Sun, W.B. Zhang, T.Y. Chen and Q.F. Zhang, *Sens. Actuators, B*, 2010, **148**, 399.
4 X. Chu, S. Zhou, W. Zhang and H. Shui, *Mater. Sci. Eng., B,* 2009, **164** , 65.
5 H.S. Woo, C.W. Na, I.D. Kim and J.H. Lee, *Nanotechnology*, 2012, **23**, 245501.
6 Y. Ding, J.Y. Shi, W.X. Wu, J. Yin and Y.X. Chen, *J. Hazard. Mater.*, 2007, **143**, 341
7 I. Guest, D.R. Varma, *J. Toxicol. Env. Health, Part A*, 1992, **36**, 27-41.
8 R. Pandeeswari and B.G. Jeyaprakash, *Biosens. Bioelectron.*, 2014, **53**, 182.
9 H.X. Tang, M. Yan, X.F. Ma, H. Zhang, M. Wang and D.R. Yang, *Sens. Actuators, B.*, 2006, **113**, 324.
10 M. Tong, G. Dai and D. Gao, *Mater. Chem. Phys.*, 2001, **69**, 176.
11 S.G. Zhao, P.G. Wei and S.H. Chen, *Sens. Actuators, B*, 2000, **62**, 117.
12 J. Zheng, G. Li, X. Ma, Y. Wang, G. Wu and Y. Cheng, *Sens. Actuators, B*, 2008, **133**, 374.
13 X.F. Lu, Q.Y. Yu, K. Wang, L.C. Shi, X. Liu, A.G. Qiu, L. Wang and D.L. Cui, *Cryst. Res. Technol.*, 2010, **45**, 557.
14 C. Luo, D. Li, W. Wu, Y. Zhang and C. Pan, *RSC Advances*, 2014, **4**, 3090.
15 C. Mondal, M. Ganguly, A. K. Sinha, J. Pal and T. Pal, *RSC Advances*, 2013, 3, 5937.
16 S. Lu, J. Qi, Z. Wang, P. Lin, S. Liu and Y. Zhang, *RSC Advances*, 2013, **3**, 19375.
17 M. G. Nair, M. Nirmala, K. Rekha and A. Anukaliani, *Mater. Lett.*, 2011, **65**, 1797.
18 W. Park, G. Jo, W.-K. Hong, J. Yoon, M. Choe, S. Lee, Y. Ji, G. Kim, Y. H. Kahng and K. Lee, *Nanotechnology*, 2011, **22**, 205204.
19 S. Panigrahi and D. Basak, *Nanoscale*, 2011, **3**, 2336.
20 S. H. Ko, D. Lee, H. W. Kang, K. H. Nam, J. Y. Yeo, S. J. Hong, C. P. Grigoropoulos and H. J. Sung, *Nano lett.*, 2011, **11**, 666.
21 X. J. Zheng, X. Cao, J. Sun, B. Yuan, Q. Li, Z. Zhu and Y. Zhang, *Nanotechnology*, 2011, **22**, 435501.
22 K. T. Park, F. Xia, S. W. Kim, S. B. Kim, T. Song, U. Paik and W. I. Park, *J. Phys. Chem. C*, 2013, **117**, 1037.
23 M. Chen, Z. Wang, D. Han, F. Gu and G. Guo, *J. Phys. Chem. C*, 2011, **115**, 12763.
24 P. Rai, Y.-S. Kim, H.-M. Song, M.-K. Song and Y.-T. Yu, *Sens. Actuators, B*, 2012, **165**, 133.
25 C. W. Na, S.-Y. Park and J.-H. Lee, *Sens. Actuators, B*, 2012, **174**, 495.
26 L. Wang, S. Wang, M. Xu, X. Hu, H. Zhang, Y. Wang and W. Huang, *Phys. Chem. Chem. Phys.*, 2013, **15**, 17179.
27 S.-L. Zhang, J.-O. Lim, J.-S. Huh, J.-S. Noh and W. Lee, *Curr. Appl. Phys.*, 2013, **13**, S156.
28 W. Tang and J. Wang, *Sens. Actuators, B*, 2015, **207**, 66.
29 H. Han, Y. Ni and E. Sheng, *RSC Advances*, 2015, **5**, 51750-51761.
30 R. Yousefi, *CrystEngComm*, 2015, **17**, 2698-2704.
31 F. Fan, Y. Feng, S. Bai, J. Feng, A. Chen and D. Li, *Sens. Actuators, B*, 2013, **185**, 377.
32 K. Gurav, M. Gang, S. Shin, U. Patil, P. Deshmukh, G. Agawane, M. Suryawanshi, S. Pawar, P. Patil and C. Lokhande, *Sens. Actuators, B*, 2014, **190**, 439.
33 S. Park, S. An, H. Ko, C. Jin and C. Lee, *ACS Appl. Mater. Interfaces*, 2012, **4**, 3650.
34 A. Katoch, G.-J. Sun, S.-W. Choi, J.-H. Byun and S. S. Kim, *Sens. Actuators, B*, 2013, **185**, 411.
35 J. Zhang, X. Liu, S. Wu, B. Cao and S. Zheng, *Sens. Actuators, B*, 2012, **169**, 61.
36 W. Guo, M. Fu, C. Zhai and Z. Wang, *Ceram. Int.*, 2014, **40**, 2295.
37 L. Wang, Z. Lou, T. Fei and T. Zhang, *J. Mater. Chem.*, 2012, **22**, 4767.
38 S. Wang, Y. Wang, H. Zhang, X. Gao, J. Yang and Y. Wang, *RSC Advances*, 2014, **4**, 30840-30849.
39 M. R. Alenezi, A. S. Alshammari, T. H. Alzanki, P. Jarowski, S. J. Henley and S. R. P. Silva, *Langmuir*, 2014, **30**, 3913-3921.
40 X. Fang, L. Hu, C. Ye and L. Zhang, *Pure Appl. Chem.*, 2010, **82**, 2185-2198.

41 M. Chen, L. Hu, J. Xu, M. Liao, L. Wu and X. Fang, *Small*, 2011, **7**, 2449-2453.
42 R. Niranjan, M. S. Londhe, A. Mandale, S. Sainkar, L. Prabhumirashi, K. Vijayamohanan and I. Mulla, *Sens. Actuators, B*, 2002, **87**, 406-413.
43 S. Hussain, T. Liu, N. Aslam, M. Kashif, S. Cao, M. Rashad, Y. Zhang, W. Zeng and M. S. Javed, *Mater. Lettr*, 2015, **152**, 260-263.
44 H. Zhang, D. Yang, D. Li, X. Ma, S. Li and D. Que, *Cryst. Growth Des.*, 2005, **5**, 547-550..
45 M. Huang, S. Weng, B. Wang, J. Hu, X. Fu and P. Liu, J. *Phys.Chem. C*, 2014, **118**, 25434-25440.
46 R. Zhang, L. Wang, J. Deng, T. Zhou, Z. Lou and T. Zhang, *Sens. Actuators, B*, 2015, **220**, 1224-1231.
47 K. Subbulakshmi, R. Pandeeswari and B. Jeyaprakash, *Superlattices Microstruct.*, 2014, **65**, 219-226.
48 Z. Lou, F. Li, J. Deng, L. Wang and T. Zhang, *ACS Appl. Mater. Interfaces*, 2013, **5**, 12310-12316.
49 R. Niranjan, M. S. Londhe, A. Mandale, S. Sainkar, L. Prabhumirashi, K. Vijayamohanan and I. Mulla, *Sens. Actuators, B*, 2002, **87**, 406-413.
50 M. Tong, G. Dai and D. Gao, *Mater. Chem. Phys.*, 2001, **69**, 176-179.
51 C.-M. Chang, M.-H. Hon and C. Leu, *RSC Advances*, 2012, **2**, 2469.
52 Q. Yu, C. Yu, J. Wang, F. Guo, S. Gao, S. Jiao, H. Li, X. Zhang, X. Wang and H. Gao, *RSC Advances*, 2013, **3**, 16619.
53 N. BARSAN and U. WEIMAR, *J. Electroceram.*, 2001, **7**, 143.
54 Y.F. Sun, S.B. Liu, F.L. Meng, J.Y. Liu, Z. Jin, L.T. Kong and J.H. Liu, *Sensors*, 2012, **12**, 2610.